

Exploiting Sparse Semantic HD Maps for Self-Driving Vehicle Localization

Wei-Chiu Ma^{*,1,2}, Ignacio Tartavull^{*,1}, Ioan Andrei Bârsan^{*,1,3}, Shenlong Wang^{*,1,3}
 Min Bai^{1,3}, Gellert Mattyus¹, Namdar Homayounfar^{1,3}, Shrinidhi Kowshika Lakshmikanth¹
 Andrei Pokrovsky¹, Raquel Urtasun^{1,3}

Abstract—In this paper we propose a novel semantic localization algorithm that exploits multiple sensors and has precision on the order of a few centimeters. Our approach does not require detailed knowledge about the appearance of the world, and our maps require orders of magnitude less storage than maps utilized by traditional geometry- and LiDAR intensity-based localizers. This is important as self-driving cars need to operate in large environments. Towards this goal, we formulate the problem in a Bayesian filtering framework, and exploit lanes, traffic signs, as well as vehicle dynamics to localize robustly with respect to a sparse semantic map. We validate the effectiveness of our method on a new highway dataset consisting of 312km of roads. Our experiments show that the proposed approach is able to achieve 0.05m lateral accuracy and 1.12m longitudinal accuracy on average while taking up only 0.3% of the storage required by previous LiDAR intensity-based approaches.

I. INTRODUCTION

High-definition maps (HD maps) are a fundamental component of most self-driving cars, as they contain useful information about the static part of the environment. The locations of lanes, traffic lights, cross-walks, as well as the associated traffic rules are typically encoded in the maps. They encode the prior knowledge about any scene the autonomous vehicle may encounter.

In order to be able to exploit HD maps, self-driving cars have to localize themselves with respect to the map. The accuracy requirements in localization are very strict and only a few centimeters of error are tolerable in such safety-critical scenarios. Over the past few decades, a wide range of localization systems has been developed. The Global Positioning System (GPS) exploits triangulation from different satellites to determine a receiver’s position. It is typically affordable, but often has several meters of error, particularly in the presence of skyscrapers and tunnels. The inertial measurement unit (IMU) computes the vehicle’s acceleration, angular rate as well as magnetic field and provides an estimate of its relative motion, but is subject to drift over time.

To overcome the limitations of GPS and IMU, place recognition techniques have been developed. These approaches store what the world looks like either in terms of geometry (e.g., LiDAR point clouds), visual appearance (e.g., SIFT

features, LiDAR intensity), and/or semantics (e.g., semantic point cloud), and formulate localization as a retrieval task. Extensions of classical methods such as iterative closest point (ICP) are typically employed for geometry-based localization [1, 40]. Unfortunately, geometric approaches suffer in the presence of repetitive patterns that arise frequently in scenarios such as highways, tunnels, and bridges. Visual recognition approaches [9] pre-record the scene and encode the “landmark” visual features. They then perform localization by matching perceived landmarks to stored ones. However, they often require capturing the same environment for multiple seasons and/or times of the day. Recent work [30] builds dense semantic maps of the environment and combines both semantics and geometry to conduct localization. However, this method requires a large amount of dense map storage and cannot achieve centimeter-level accuracy.

While place recognition approaches are typically fairly accurate, the costs associated with ensuring the stored representations are up to date can often be prohibitive. They also require very large storage on board. Several approaches have been proposed to provide affordable solutions to localization by exploiting coarse maps that are freely available on the web [8, 23]. Despite demonstrating promising results, the accuracy of such methods is still in the order of a few meters, which does not meet the requirements of safety-critical applications such as autonomous driving.

With these challenges in mind, in this paper we propose a lightweight localization method that does not require detailed knowledge about the appearance of the world (e.g., dense geometry or texture). Instead, we exploit vehicle dynamics as well as a semantic map containing lane graphs and the locations of traffic signs. Traffic signs provide information in longitudinal direction, while lanes help avoid lateral drift. These cues are complementary to each other and the resulting maps can be stored in a fraction of the memory necessary for traditional HD maps, which is important as self-driving cars need to operate in very large environments. We formulate the localization problem as a Bayes filter, and demonstrate the effectiveness of our approach on North-American highways, which are challenging for current place recognition approaches as repetitive patterns are common and driving speeds are high. Our experiments on more than 300 km of testing trips showcase that we are able to achieve 0.05m median lateral accuracy and 1.12m median longitudinal accuracy, while using roughly three orders of

* Equal contribution

¹ Uber Advanced Technologies Group

² Department of Electrical Engineering and Computer Science, MIT

³ Department of Computer Science, University of Toronto

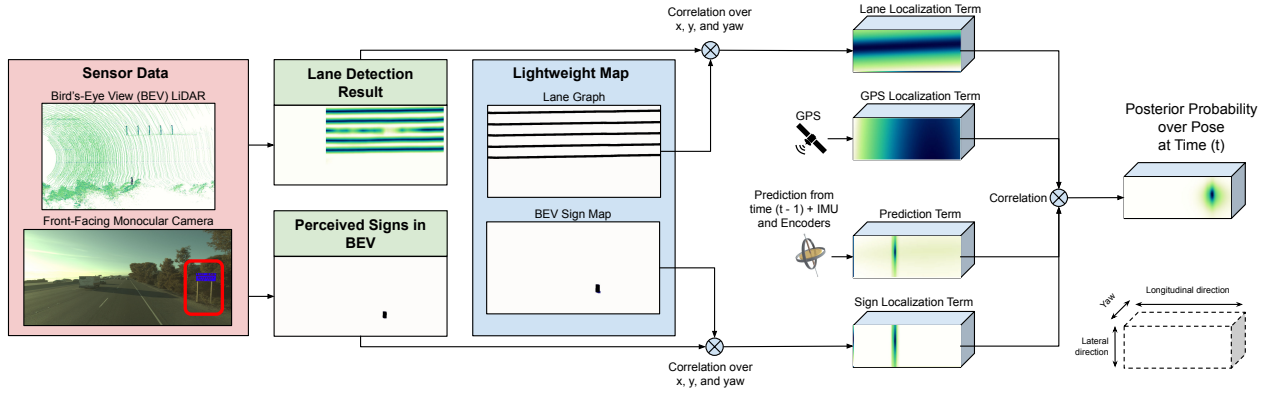


Fig. 1: **System architecture.** Given the camera image and LiDAR sweep as input, we first detect lanes in the form of truncated inverse distance transform and detect signs as a bird’s-eye view (BEV) probability map. The detection output is then passed through a differentiable rigid transform layer [14] under multiple rotational angles. Finally, the inner-product score is measured between the inferred semantics and the map. The probability score is merged with GPS and vehicle dynamics observations and the inferred pose is computed from the posterior using soft-argmax. The camera image on the left contains an example of a sign used in localization, highlighted with the red box.

magnitude less storage than previous map-based approaches (0.55MiB/km² vs. the 1.4GiB/km² required for dense point clouds).

II. RELATED WORK

Place Recognition: One of the most prevailing approaches in self-localization is place recognition [2, 3, 6, 13, 20, 25, 29, 38, 41]. By recording the appearance of the world and building a database of it in advance, the localization task can be formulated as a retrieval problem. At test time, the system simply searches for the most similar scene and retrieves its pose. As most of the features used to describe the scene (e.g., 3D line segments [6] or 3D point clouds [20, 25, 38]), are highly correlated with the appearance of the world, one needs to update the database frequently. With this problem in mind, [9, 21, 27] proposed an image-based localization technique that is to some degree invariant to appearance changes. More recently, [15] designed a CNN to directly estimate the pose of the camera. While their method is robust to illumination changes and weather, they still require training data for each scene, limiting its scalability.

Geometry-based Localization: Perspective-n-Point (PnP) approaches have been used for localization. The idea is to extract local features from images and find correspondences with the pre-stored geo-registered point sets. For instance, [32] utilized random forests to find correspondence between RGBD images and pre-constructed 3D indoor geometry. Li et al. [20] pre-stored point clouds along with SIFT features for this task, while Liu et al. [22] proposed to use branch-and-bound to solve the exact 2D-3D registration. However, these approaches require computing a 3D reconstruction of the scene in advance, and do not work well in scenarios with repetitive geometric structures.

Simultaneous Localization and Mapping: Given a sequence of images, point clouds, or depth images, SLAM approaches [10, 26, 42] estimate relative camera poses between consecutive frames through feature matching and joint

pose estimation. Accumulated errors make the localization gradually drift as the robot moves. In indoor or urban scenes, loop closure has been used to fix the accumulated errors. However, unlike indoor or urban scenarios, on highways trajectories are unlikely to be closed, which makes drift a much more challenging problem to overcome.

Lightweight Localization: There is a growing interest in developing affordable localization techniques. Given an initial estimate of the vehicle position, [11] exploited ego-trajectory to self-localize within a small region. Brubaker et al. [8] developed a technique that can be applied at city scale, without any prior knowledge about the vehicle location. Ma et al. [23] incorporated other visual cues, such as the position of the sun and the road type to further improve the results. These works are appealing since they only require a cartographic map. However, the localization accuracy is strongly limited by the performance of odometry. The semantic cues are only used to resolve ambiguous modes and speed up the inference procedure. Second, the computational complexity is a function of the uncertainty in the map, which remains fairly large when dealing with maps that have repetitive structures.

High-precision Map-based Localization: The proposed work belongs to the category of the high-precision map-based localization [7, 18, 19, 31, 38, 39, 40, 44]. The use of maps has been shown to not only provide strong cues for various tasks in computer vision and robotics such as scene understanding [34], vehicle detection [24], and localization [8, 23, 35], but also enables the creation of large-scale datasets with little human effort [33, 36]. The general idea is to build a centimeter-level high-definition 3D map offline a priori, by stitching sensor input using a high-precision differential GNSS system and offline SLAM. Early approaches utilize LiDAR sensors to build maps [18]. Uncertainty in intensity changes have been handled through building probabilistic prior map [19, 39]. In the online stage, the position is determined by matching the sensor reading

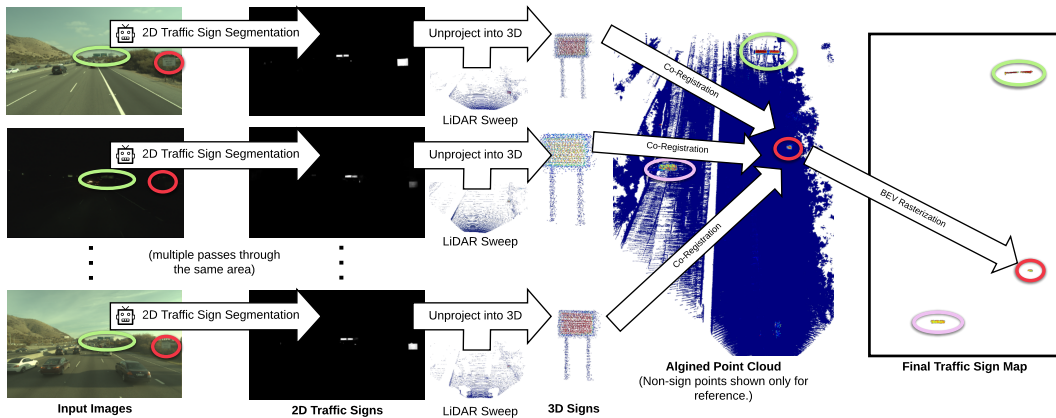


Fig. 2: **Traffic sign map building process.** We first detect signs in 2D using semantic segmentation in the camera frame, and then use the LiDAR points to localize the signs in 3D. Mapping can aggregate information from multiple passes through the same area using the ground truth pose information, and can function even in low light, as highlighted in the middle row, where the signs are correctly segmented even at night time. This information is used to build the traffic sign map in a fully automated way.

to the prior map. For instance, [18, 19, 39] utilized the perceived LiDAR intensity to conduct matching. Yoneda et al. [40] proposed to align online LiDAR sweeps against an existing 3D prior map using ICP, [38, 44] utilized visual cues from cameras to localize the self-driving vehicles, and [7] use a fully convolutional neural network to learn the task of online-to-map matching in order to improve robustness to dynamic objects and eliminate the need for LiDAR intensity calibration.

Semantic Localization: Schreiber et al. [31] proposed to use lanes as localization cues. Towards this goal, they manually annotated lane markings over the LiDAR intensity map. The lane markings are then detected online using a stereo camera, and matched against the ones in the map. Welzel et al. [37] and Qu et al. [28] utilize traffic signs to assist image-based vehicle localization. Specifically, traffic signs are detected from images and matched against a geo-referenced sign database, after which local bundle adjustment is conducted to estimate a fine-grained pose. More recently, [30] built dense semantic maps using image segmentation and conducted localization by matching both semantic and geometric cues. In contrast, the maps used in our approach only need to contain the lane graphs and the inferred sign map, the latter of which is computed without a human in the loop, while also only requiring a fraction of the storage used by dense maps.

III. LIGHTWEIGHT HD MAPPING

In order to conduct efficient and accurate localization, a compressed yet informative representation of the world needs to be constructed. Ideally our HD maps should be easy to (automatically) build and maintain at scale, while also enabling real-time broadcasting of map changes between a central server and the fleet. This places stringent storage requirements that traditional dense HD maps fail to satisfy. In this paper, we tackle these challenges by building sparse HD maps containing just the lane graph and the locations

of traffic signs. These modalities provide complementary semantic cues for localization. Importantly, the storage needs for our maps are three orders of magnitude smaller than traditional LiDAR intensity maps [7, 18, 19, 39] or geometric maps [40].

a) Lane Graph: Most roads have visually distinctive lanes determining the expected trajectory of vehicles, compliant with the traffic rules. Most self driving cars store this prior knowledge as lane graphs \mathcal{L} . A lane graph is a structured representation of the road network defined as a set of polygonal chains (polylines), each of which represents a lane boundary. We refer the reader to Fig. 1 for an illustration of a lane graph. Lane graphs provide useful cues for localization, particularly in the lateral position and the heading of the vehicle.

b) Traffic Signs: Traffic signs are common semantic landmarks that are sparsely yet systematically present in cities, rural areas, and highways. Their presence provides useful cues that can be employed for accurate longitudinal localization. In this paper we build sparse HD maps containing traffic signs automatically. Towards this goal, we exploit multiple passes of our vehicles over the same region and identify the signs by exploiting image-based semantic segmentation followed by 3D sign localization using LiDAR via inverse-projection from pixel to 3D space. A consistent coordinate system over the multiple passes is obtained by means of offline multi-sensor SLAM. Note that in our map we only store points that are estimated to be traffic signs above a certain confidence level. After that, we rasterize the sparse points to create the traffic sign presence probability map \mathcal{T} in bird’s-eye view (BEV) at 5cm per pixel. This is a very sparse representation containing all the traffic signs. The full process is conducted without any human intervention. Fig. 2 depicts the traffic sign map building process and an example of its output.

IV. LOCALIZATION AS BAYES INFERENCE WITH DEEP SEMANTICS

In this paper we propose a novel localization system that exploits vehicle dynamics as well as a semantic map containing both a lane graph and the locations of traffic signs. These cues are complementary to each other and the resulting maps can be stored in a fraction of the memory necessary for traditional dense HD maps. We formulate the localization problem as a histogram filter taking as input the structured outputs of our sign and lane detection neural networks, as well as GPS, IMU, and wheel odometry information, and outputting a probability histogram over the vehicle's pose, expressed in world coordinates.

A. Probabilistic Pose Filter Formulation

Our localization system exploits a wide variety of sensors: GPS, IMU, wheel encoders, LiDAR, and cameras. These sensors are available in most self-driving vehicles. The GPS provides a coarse location with several meters accuracy; an IMU captures vehicle dynamic measurements; the wheel encoders measure the total travel distance; the LiDAR accurately perceives the geometry of the surrounding area through a sparse point cloud; images capture dense and rich appearance information. We assume our sensors are calibrated and neglect the effects of suspension, unbalanced tires, and vibration. As shown in our experiments, the influence of these factors is negligible and other aspects such as sloped roads (e.g., on highway ramps) do not have an impact on our localizer. Therefore, the vehicle's pose can be parametrized with only three degrees of freedom (instead of six) consisting of a 2D translation and a heading angle w.r.t. the map coordinate's origin, i.e. $\mathbf{x} = \{\mathbf{t}, \theta\}$, where $\mathbf{t} \in \mathbb{R}^2$ and $\theta \in (-\pi, \pi]$, since the heading is parallel to the ground plane.

Following similar concepts to [7], we factorize the posterior distribution over the vehicle's pose into components corresponding to each modality, as shown in Equation (1).

Let \mathcal{G}_t be the GPS readings at time t and let \mathcal{L} and \mathcal{T} represent the lane graph and traffic sign maps respectively. We compute an estimate of the vehicle dynamics \mathcal{X}_t from both IMU and the wheel encoders smoothed through an extended Kalman filter, which is updated at 100Hz.

The localization task is formulated as a histogram filter aiming to maximize the agreement between the observed and mapped lane graphs and traffic signs while respecting vehicle dynamics:

$$\text{Bel}_t(\mathbf{x}) = \eta \cdot P_{\text{LANE}}(\mathcal{S}_t | \mathbf{x}, \mathcal{L}; \mathbf{w}_{\text{LANE}}) P_{\text{SIGN}}(\mathcal{S}_t | \mathbf{x}, \mathcal{T}; \mathbf{w}_{\text{SIGN}}) P_{\text{GPS}}(\mathcal{G}_t | \mathbf{x}) \text{Bel}_{t-1}(\mathbf{x} | \mathcal{X}_t), \quad (1)$$

where $\text{Bel}_t(\mathbf{x})$ is the posterior probability of the vehicle pose at time t ; η is a normalizing factor to ensure sum of all probability is equal to one; \mathbf{w}_{LANE} and \mathbf{w}_{SIGN} are sets of learnable parameters, and $\mathcal{S}_t = (\mathcal{I}_t, \mathcal{C}_t)$ is a sensory measurement tuple composed from LiDAR \mathcal{I}_t and camera \mathcal{C}_t . Note that by recursively solving Eq. (1), we can localize the vehicle at every step with an uncertainty measure that

could be propagated to the next step. We now describe each energy term and our inference algorithm in more detail.

a) *Lane Observation Model*: We define our matching energy to encode the agreement between the lane observation from the sensory input and the map. Our probability is computed by a normalized matching score function that utilizes the existing lane graph and compares it to detected lanes. To detect lanes we exploit a state-of-the-art real-time multi-sensor convolutional network [4]. The input of the network is a front-view camera image and raw LiDAR intensity measurement projected onto BEV. The output of the network is the inverse truncated distance function to the lane graph in the overhead view. Specifically, each pixel in the overhead view encodes the Euclidean distance to the closest lane marking, up to a truncation threshold of 1m. We refer the reader to Fig. 3 for an illustration of the neural network's input and output.

To compute the probability, we first orthographically project the lane graph \mathcal{L} onto overhead view such that the lane detection output and the map are under the same coordinate system. The overhead view of the lane graph is also represented using an truncated inverse distance function. Given a vehicle pose hypothesis \mathbf{x} , we rotate and translate the lane detection prediction accordingly and compute its matching score against the lane graph map. The matching score is an inner product between the lane detection and the lane graph map

$$P_{\text{LANE}} \propto s(\pi(f_{\text{LANE}}(\mathcal{S}; \mathbf{w}_{\text{LANE}}), \mathbf{x}), \mathcal{L}), \quad (2)$$

where f_{LANE} is the deep lane detection network and \mathbf{w}_{LANE} are the network's parameters. π is a 2D rigid transform function to transform the online lane detection to the map's coordinate system given a pose hypothesis \mathbf{x} ; $s(\cdot, \cdot)$ is a cross-correlation operation between two images.

b) *Traffic Sign Observation Model*: This model encodes the consistency between perceived online traffic signs and the map. Specifically, we run an image-based semantic segmentation algorithm that performs dense semantic labeling of traffic signs. We adopt the state-of-the-art PSPnet structure [43] to our task. The encoder architecture is a ResNet50 backbone and the decoder is a pyramid spatial pooling network. Two additional convolutional layers are added in the decoder stage to further boost performance. The model is jointly trained with the instance segmentation loss following [5]. Fig. 3 depicts examples of the network's input and output. The estimated image-based traffic sign probabilities are converted onto the overhead view to form our online traffic sign probability map. This is achieved by associating each LiDAR with a pixel in the image by projection. We then read the softmax probability of the pixel's segmentation as our estimate. Only high-confident traffic sign pixels are unprojected to 3D and rasterized in BEV. Given a pose proposal \mathbf{x} , we define the sign matching probability analogously to the lane matching one as

$$P_{\text{SIGN}} \propto s(\pi(f_{\text{SIGN}}(\mathcal{S}; \mathbf{w}_{\text{SIGN}}), \mathbf{x}), \mathcal{T}), \quad (3)$$

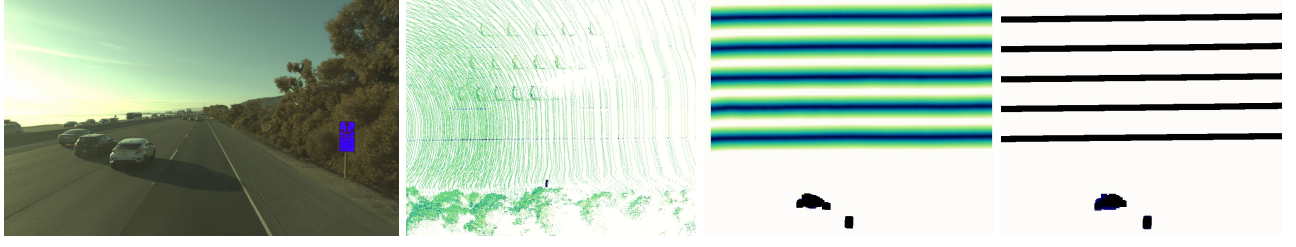


Fig. 3: **Dataset sample and inference results.** Our system detects signs in the camera images (note the blue rectangle on the right side of the first image) and projects the sign’s points in a top-down view using LiDAR (second image). It uses this result in conjunction with the lane detection result (third image) to localize against a lightweight map consisting of just signs and lane boundaries (fourth image).

where f_{SIGN} is the sign segmentation network and \mathbf{w}_{SIGN} are the networks’ parameters. Both the perceived signs, as well as the map they are matched against are encoded as pixel-wise occupancy probabilities.

c) *GPS Observation Model:* This term encodes the likelihood of the GPS sensory observation \mathcal{G} at a given vehicle pose \mathbf{x} :

$$P_{\text{GPS}} \propto \exp \left(-\frac{(g_x - x)^2 + (g_y - y)^2}{\sigma_{\text{GPS}}^2} \right), \quad (4)$$

where $[g_x, g_y]^T = T \cdot \mathcal{G}$ represents a GPS point location in the coordinate frame of the map against which we are localizing. T is the given rigid transform between the Universal Transverse Mercator (UTM) coordinates and the map coordinates and \mathcal{G} is the GPS observation expressed in UTM coordinates.

d) *Dynamics Model:* This term encourages consistency between the pose proposal \mathbf{x} and the vehicle dynamics estimation, given the previous vehicle pose distribution. The pose at the current timestamp depends on previous pose and the vehicle motion. Given an observation of the vehicle motion \mathcal{X}_t , the motion model is computed by marginalizing out the previous pose:

$$\text{Bel}_{t|t-1}(\mathbf{x}|\mathcal{X}_t) = \sum_{\mathbf{x}_{t-1} \in \mathcal{R}_{t-1}} P(\mathbf{x}|\mathcal{X}_t, \mathbf{x}_{t-1}) \text{Bel}_{t-1}(\mathbf{x}_{t-1}) \quad (5)$$

where the likelihood is a Gaussian probability model

$$P(\mathbf{x}|\mathcal{X}_t, \mathbf{x}_{t-1}) \propto \mathcal{N}((\mathbf{x} \ominus (\mathbf{x}_{t-1} \oplus \mathcal{X}_t)), \Sigma) \quad (6)$$

with Σ the covariance matrix and \mathcal{R}_{t-1} is the search space for \mathbf{x}_{t-1} . In practice, we only need \mathcal{R}_{t-1} to be a small local region centered at \mathbf{x}_{t-1}^* given the fact the rest of the pose space has negligible probability. Note that \oplus, \ominus are the standard 2D pose composition and inverse pose composition operators described by Kummerle et al. [17].

B. Efficient Inference

a) *Discretization:* The inference defined in Eq. (1) is intractable. Following [7, 19] we tackle this problem using a histogram filter. We discretize the full continuous search space over $\mathbf{x} = \{x, y, \theta\}$ into a search grid, each with associated posterior $\text{Bel}(\mathbf{x})$. We restrict the search space to a small local region at each time. This is a reasonable assumption given the constraints of the vehicles dynamics at a limited time interval.

b) *Accelerating Correlation:* We now discuss the computation required for each term. We utilize efficient convolution-based exhaustive search to compute the lane and traffic sign probability model. In particular, enumerating the full translational search range with inner product is equivalent to a correlation filter with a large kernel (which is the online sign/lane observation). Motivated by the fact that the kernel is very large, FFT-conv is used to accelerate the computation speed by a factor of 20 over the state-of-the-art GEMM-based spatial GPU correlation implementations [7].

c) *Robust Point Estimation:* Unlike the MAP-inference which simply takes the configuration which maximizes the posterior belief, we adopt a center-of-mass based soft-argmax [19] to better incorporate the uncertainty of our model and encourage smoothness in our localization. We thus define

$$\mathbf{x}_t^* = \frac{\sum_{\mathbf{x}} \text{Bel}_t(\mathbf{x})^\alpha \cdot \mathbf{x}}{\sum_{\mathbf{x}} \text{Bel}_t(\mathbf{x})^\alpha}, \quad (7)$$

where $\alpha \geq 1$ is a temperature hyper-parameter. This gives us an estimate that takes the uncertainty of the prediction into account.

C. Learning

Both the lane detection network and the traffic sign segmentation network are trained through back-propagation separately using ground-truth annotated data. The lane detection is trained with a regression loss that measures the ℓ_2 distance between the predicted inverse truncated distance transform and the ground-truth one [4]. The semantic segmentation network is trained with cross-entropy [5]. Hyper-parameters for the Bayes filter (e.g., σ_{GPS}^2 , softmax temperature α , etc.) are searched through cross-validation.

V. EXPERIMENTS

We validate the effectiveness of our localization system on a highway dataset of 312km. We evaluate our model in terms of its localization accuracy and runtime.

A. Dataset

Our goal is to perform fine-grained localization on highways. Unfortunately, there is no publicly available dataset that provides ground truth localization at the centimeter-level precision required for safe autonomous driving. We therefore collected a dataset of highways by driving over 300km in North America at different times of the year, covering over

100km of roads. The dataset encompasses 64-line LiDAR sweeps and images from a front-facing global shutter camera with a resolution of 1900×1280 , both captured at 10Hz, as well as IMU and GPS sensory data and the lane graphs. The extrinsic calibration between the camera and LiDAR is conducted using a set of calibration targets [12]. The ground truth 3D localization is estimated by a high-precision ICP-based offline Graph-SLAM using high-definition pre-scanned scene geometry. Fig. 3 shows a sample from our dataset together with the inferred and ground truth lane graphs.

Our dataset is partitioned into ‘snippets’, each consisting of roughly 2km of driving. The training, validation, and test splits are conducted at the snippet level, where training snippets are used for map building and training the lane detection network, and validation snippets are used for hyper-parameter tuning. The test snippets are used to compute the final metrics. An additional 5,000 images have been annotated with pixel-wise traffic sign labels which are used for training the sign segmentation network.

B. Implementation Details

Network Training: To train the lane detection network, we uniformly sample 50K frames from the training region based on their geographic coordinates to train the network. The ground truth can be automatically generated given the vehicle pose and the lane graph. We use a mini-batch size of 16 and employ Adam [16] as the optimizer. We set the learning rate to 10^{-4} . The network was trained completely from scratch with Gaussian initialization and converged roughly after 10 epochs. We visualize some results in Fig. 3.

We train our traffic sign segmentation network separately over four GPUs with a total mini-batch size of 8. Synchronized batch normalization is utilized for multi-GPU batch normalization. The learning rate is set to be 10^{-4} and the network is trained from scratch. The backbone of the model is fine-tuned from a DeepLab v2 network pre-trained over the Pascal VOC dataset.

Hyper-parameter Search: We choose the hyper-parameters through grid search over a mini-validation dataset consists of 20 snippets of 2km driving. The hyper-parameters include the temperatures of the final pose soft-argmax, the lane probability softmax, and the sign probability softmax, as well as the observation noise parameters for GPS and the dynamics. The best configuration is chosen by the failure rate metric. In the context of hyperparameter search, the failure rate is a snippet-level metric which counts a test snippet as failed if the total error becomes greater than 1m at any point. We therefore picked the hyperparameter configuration which minimized this metric on our validation set, and kept it fixed at test time. As noted in Sec. IV-B, we restrict our search range to a small area centered at the dead reckoning pose and neglect the probability outside the region. We notice in practice that thanks to the consistent presence of the lanes in self-driving scenarios, there is less uncertainty along the lateral direction than along the longitudinal. The presence of traffic signs helps reduce uncertainty along the longitudinal direction, but signs could be as sparse as every 1km, during

which INS drift could be as large as 7 meters. Based on this observation and with the potential drift in mind, we choose a very conservative search range $B = B_x \times B_y \times B_\theta = [-0.75m, 0.75m] \times [-7.5m, 7.5m] \times [-2^\circ, 2^\circ]$ at a spatial resolution of 5cm and an angular resolution of 1° .

C. Localization

Metrics: We adopt several key metrics to measure the localization performance of the algorithms evaluated in this Section.

In order to safely drive from a certain point to another without any human intervention, an autonomous vehicle must be aware of where it is w.r.t. the map. Lateral error and longitudinal error have different meanings for self-driving since a small lateral error could result in localizing in the wrong lane, while ambiguities about the longitudinal position of the vehicle are more tolerable. As localization is the first stage in self-driving pipeline, it is critical that it is robust enough with a very small failure rate; therefore, understanding worst-case performance is critical.

Moreover, localization results should reflect the vehicle dynamics as well, which ensures the smoothness of decision making, since sudden jumps in localization might cause downstream components to fail. To this end, we also measure the prediction smoothness of our methods. We define smoothness as the difference between the temporal gradient of the ground truth pose and that of the predicted pose. We estimate the gradients using first-order finite differences, i.e., by simply taking the differences between poses at times (t) and $(t - 1)$. As such, we define smoothness as

$$s = \frac{1}{T} \sum_{t=1}^T \left\| (\mathbf{x}_t^* - \mathbf{x}_{t-1}^*) - (\mathbf{x}_t^{GT} - \mathbf{x}_{t-1}^{GT}) \right\|^2. \quad (8)$$

Baselines: We compare our results with two baselines: dynamics and dynamics+GPS. The first baseline builds on top of the dynamics of the vehicle. It takes as input the IMU data and wheel odometry, and use the measurements to extrapolate the vehicle’s motion. The second baseline employs histogram filters to fuse information between IMU readings and GPS sensory input, which combines motion and absolute position cues.

Quantitative Analysis: As shown in Tab. I and II, our method significantly outperforms the baselines across all metrics. To be more specific, our model has a median longitudinal error of 1.12m and a median lateral error of 0.06m; both are much smaller than other competing methods, with lateral error one order of magnitude lower. We notice that our method greatly improve the performance over the worst case scenario in terms of both longitudinal error, lateral error, and smoothness.

Qualitative Results: We show the localization results of our system as well as those of the baselines in Fig. 4. Through lane observations, our model is able to consistently achieve centimeter-level lateral localization accuracy. When signs are visible, the traffic sign model helps push the prediction towards the location where the observation

TABLE I: Quantitative results on localization accuracy. Here, ‘Ours’ refers to the model proposed in this paper using dynamics, GPS, lanes, and signs, in a probabilistic framework.

Methods	Longitudinal Error (m)			Lateral Error (m)		
	Median	95%	99%	Median	95%	99%
Dynamics	24.85	128.21	310.50	114.46	779.33	784.22
GPS	1.16	5.78	6.76	1.25	8.56	9.44
INS	1.59	6.89	13.62	2.34	11.02	42.34
Ours	1.12	3.55	5.92	0.05	0.18	0.23

TABLE II: Quantitative results on smoothness

Method Name	Smoothness			
	Mean	95%	99%	Max
Dynamics	0.2	0.4	0.6	1.2
GPS	0.1	0.2	0.3	8.5
INS	0.1	0.1	0.2	3.7
Ours	0.1	0.2	0.3	0.9

and map have agreement, bringing the pose estimate to the correct longitudinal position. In contrast, GPS tends to produce noisy results, but helps substantially improve worst-case performance.

Runtime Analysis: To further demonstrate that our localization system is of practical usage, we benchmark the runtime of each component in the model during inference using an NVIDIA GTX 1080 GPU. A single step of our inference takes 153ms in total on average, with 32ms on lane detection, 110ms on semantic segmentation and 11ms on matching, which is roughly 7 fps. We note that the real-time performance is made possible largely with the help of FFT convolutions.

Map Storage Analysis: We compare the size of our HD map against other commonly used representations: LiDAR intensity map and 3D point cloud map. For a fair comparison, we store all data in a lossless manner and measure the storage requirements. While the LiDAR intensity and 3D point cloud maps consume 177 MiB/km² and 1,447 MiB/km² respectively, our HD map only requires **0.55 MiB** per square kilometer. This is only 0.3% of the size of LiDAR intensity map and 0.03% of that of 3D point cloud map.

Ablation Study: To better understand the contribution of each component of our model, we respectively compute the longitudinal and lateral error under diverse settings. As shown in Tab. III, each term (GPS, lane, sign) has a positive contribution to the localization performance. Specifically, the lane observation model greatly increases lateral accuracy, while sign observations increase longitudinal accuracy. We also compare our probabilistic histogram filter formulation with a deterministic model. Compared against our histogram filter approach, the non-probabilistic one performs a weighted average between each observation without carrying over the previous step’s uncertainty. As shown in Tab. IV, by combining all the observation models, the non-probabilistic model can achieve reasonable performance but still remains less accurate than the probabilistic formulation. Moreover, due to the fact that no uncertainty history is carried over, prediction smoothness over time is not guaranteed.

VI. CONCLUSION

In this paper we proposed a robust localization system capable of localizing an autonomous vehicle against a map requiring roughly three orders of magnitude less storage than traditional methods. This has the potential to substantially improve the scalability of self-driving technologies by reducing storage costs, while also enabling map updates to be delivered to vehicles at vastly reduced costs.

We approached the task by identifying two sets of complementary cues capable of disambiguating the lateral and longitudinal position of the vehicle: lane boundaries and traffic signs. We integrated these cues into a pipeline alongside GPS, IMU, and wheel encoders, and showed that the system is able to run in real time at roughly 7Hz on a single GPU. We demonstrated the efficacy of our method on a large-scale highway dataset consisting of over 300km of driving, showing that it can achieve the localization accuracy requirements of self-driving cars, while using much less storage.

REFERENCES

- [1] F. Aghili and C. Y. Su. Robust relative navigation by integration of ICP and adaptive Kalman filter using laser scanner and IMU. *TMECH*, 2016.
- [2] R. Arandjelovic, P. Gronat, A. Torii, T. Pajdla, and J. Sivic. NetVLAD: CNN architecture for weakly supervised place recognition. *IEEE TPAMI*, 2017.
- [3] G. Baatz, K. Köser, D. Chen, R. Grzeszczuk, and M. Pollefeys. Leveraging 3D City Models for Rotation Invariant Place-of-Interest Recognition. *IJCV*, 2012.
- [4] M. Bai, G. Mattyus, N. Homayounfar, S. Wang, S. Lakshminanth, and R. Urtasun. Deep multi-sensor lane detection. In *IROS*, 2018.
- [5] M. Bai and R. Urtasun. Deep watershed transform for instance segmentation. In *CVPR*. IEEE, 2017.
- [6] M. Bansal and K. Daniilidis. Geometric urban geo-localization. In *CVPR*, 2014.
- [7] I. A. Bărsan, S. Wang, A. Pokrovsky, and R. Urtasun. Learning to localize using a lidar intensity map. In *CoRL*, 2018.
- [8] M. Brubaker, A. Geiger, and R. Urtasun. Lost! leveraging the crowd for probabilistic visual self-localization. In *CVPR*, 2013.
- [9] M. Cummins and P. Newman. Fab-map: Probabilistic localization and mapping in the space of appearance. *IJRR*, 2008.
- [10] J. Engel, T. Schöps, and D. Cremers. Lsd-slam: Large-scale direct monocular slam. In *ECCV*, 2014.
- [11] G. Floros, B. van der Zander, and B. Leibe. OpenStreetSLAM: Global vehicle localization using OpenStreetMaps. In *ICRA*, 2013.
- [12] R. Hartley and A. Zisserman. *Multiple view geometry in computer vision*. Cambridge university press, 2003.
- [13] J. Hays and A. A. Efros. im2gps: estimating geographic information from a single image. In *CVPR*, 2008.
- [14] M. Jaderberg, K. Simonyan, A. Zisserman, et al. Spatial transformer networks. In *NIPS*, 2015.
- [15] A. Kendall, M. Grimes, and R. Cipolla. Posenet: A convolutional network for real-time 6-dof camera relocalization. In *ICCV*, 2015.
- [16] D. P. Kingma and J. Ba. Adam: A method for stochastic optimization. *arXiv preprint arXiv:1412.6980*, 2014.
- [17] R. Kümmerle, B. Steder, C. Dornhege, M. Ruhnke, G. Grisetti, C. Stachniss, and A. Kleiner. On measuring the accuracy of slam algorithms. *Autonomous Robots*, 27(4):387, 2009.
- [18] J. Levinson, M. Montemerlo, and S. Thrun. Map-based precision vehicle localization in urban environments. In *RSS*, 2007.

TABLE III: Ablation studies on the impact of each system component

Method	Properties			Travelling Dist = 2km					
	Lane	GPS	Sign	Longitudinal Error (m)			Lateral Error (m)		
				Median	95%	99%	Median	95%	99%
Lane	yes	no	no	13.45	37.86	51.59	0.20	1.08	1.59
Lane+GPS	yes	yes	no	1.53	5.95	6.27	0.06	0.24	0.43
Lane+Sign	yes	no	yes	6.23	31.98	51.70	0.10	0.85	1.41
All	yes	yes	yes	1.12	3.55	5.92	0.05	0.18	0.23

TABLE IV: Ablation studies on inference settings with full observations (Lane+GPS+Sign)

Inference	Travelling Dist = 2km						Smoothness			
	Longitudinal Error (m)			Lateral Error (m)			Mean	95%	99%	Max
	Median	95%	99%	Median	95%	99%				
Deterministic	1.29	3.65	5.16	0.08	0.26	0.50	0.11	0.19	1.78	5.27
Probabilistic	1.12	3.55	5.92	0.05	0.18	0.23	0.07	0.19	0.24	0.98

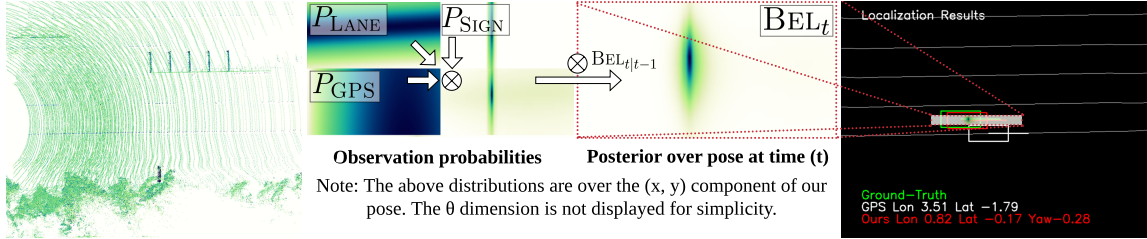


Fig. 4: **Qualitative results.** A bird's-eye view of the last five LiDAR sweeps (left), which are used for the lane detection, together with the observation probabilities and the posterior (middle), followed by a comparison between the localization result, the ground truth pose, and GPS (right). The (x, y)-resolution of each probability distribution is 1.5m laterally (vertical) and 15m longitudinally (horizontal).

- [19] J. Levinson and S. Thrun. Robust vehicle localization in urban environments using probabilistic maps. In *ICRA*, 2010.
- [20] Y. Li, N. Snavely, D. Huttenlocher, and P. Fua. Worldwide pose estimation using 3d point clouds. In *ECCV*, 2012.
- [21] C. Linegar, W. Churchill, and P. Newman. Work smart, not hard: Recalling relevant experiences for vast-scale but time-constrained localisation. In *ICRA*, 2015.
- [22] L. Liu, H. Li, and Y. Dai. Efficient global 2d-3d matching for camera localization in a large-scale 3d map. In *ICCV*, 2017.
- [23] W.-C. Ma, S. Wang, M. A. Brubaker, S. Fidler, and R. Urtasun. Find your way by observing the sun and other semantic cues. In *ICRA*, 2017.
- [24] K. Matzen and N. Snavely. Nyc3dcars: A dataset of 3d vehicles in geographic context. In *ICCV*, 2013.
- [25] F. Moosmann and C. Stiller. Joint self-localization and tracking of generic objects in 3d range data. In *ICRA*, 2013.
- [26] R. Mur-Artal and J. D. Tardos. ORB-SLAM2: An Open-Source SLAM System for Monocular, Stereo, and RGB-D Cameras. *T-RO*, 2017.
- [27] P. Nelson, W. Churchill, I. Posner, and P. Newman. From dusk till dawn: Localisation at night using artificial light sources. In *ICRA*, 2015.
- [28] X. Qu, B. Soheilian, and N. Paparoditis. Vehicle localization using mono-camera and geo-referenced traffic signs. In *IVS*. IEEE, 2015.
- [29] T. Sattler, B. Leibe, and L. Kobbelt. Fast image-based localization using direct 2d-to-3d matching. In *ICCV*, 2011.
- [30] J. Schönberger, M. Pollefeys, A. Geiger, and T. Sattler. Semantic visual localization. *JPRS*, 2018.
- [31] M. Schreiber, C. Knöppel, and U. Franke. Laneloc: Lane marking based localization using highly accurate maps. In *IV*, 2013.
- [32] J. Shotton, B. Glocker, C. Zach, S. Izadi, A. Criminisi, and A. Fitzgibbon. Scene coordinate regression forests for camera relocalization in rgb-d images. In *CVPR*, 2013.
- [33] S. Wang, M. Bai, G. Mattyus, H. Chu, W. Luo, B. Yang, J. Liang, J. Chaverie, S. Fidler, and R. Urtasun. Torontocity: Seeing the world with a million eyes. *arXiv preprint arXiv:1612.00423*, 2016.
- [34] S. Wang, S. Fidler, and R. Urtasun. Holistic 3d scene understanding from a single geo-tagged image. In *CVPR*, 2015.
- [35] S. Wang, S. Fidler, and R. Urtasun. Lost shopping! monocular localization in large indoor spaces. In *ICCV*, 2015.
- [36] J. D. Wegner, S. Branson, D. Hall, K. Schindler, and P. Perona. Cataloging public objects using aerial and street-level images-urban trees. In *CVPR*, 2016.
- [37] A. Welzel, P. Reisdorf, and G. Wanielik. Improving urban vehicle localization with traffic sign recognition. In *ICITS*. IEEE, 2015.
- [38] R. W. Wolcott and R. M. Eustice. Visual localization within lidar maps for automated urban driving. In *IROS*, 2014.
- [39] R. W. Wolcott and R. M. Eustice. Fast lidar localization using multiresolution gaussian mixture maps. In *ICRA*, 2015.
- [40] K. Yoneda, H. Tehrani, T. Ogawa, N. Hukuyama, and S. Mita. Lidar scan feature for localization with highly precise 3-d map. In *IV*, 2014.
- [41] A. R. Zamir, A. Hakeem, and R. Szeliski. *Large-Scale Visual Geo-Localization*. Springer, 2016.
- [42] J. Zhang and S. Singh. Loam: Lidar odometry and mapping in real-time. In *RSS*, 2014.
- [43] H. Zhao, J. Shi, X. Qi, X. Wang, and J. Jia. Pyramid scene parsing network. In *CVPR*, 2017.
- [44] J. Ziegler, H. Lategahn, M. Schreiber, C. G. Keller, C. Knöppel, J. Hipp, M. Haueis, and C. Stiller. Video based localization for bertha. In *IV*, 2014.